Linz-Donawitz steel slag for the removal of hydrogen sulfide at room temperature

MIGUEL A. MONTES-MORÁN,*[,1] ALEJANDRO CONCHESO,[1] CARLA CANALS-BATLLE,[2] NOELIA V. AGUIRRE,[1,3] CONCHI O. ANIA,[1] MARÍA J. MARTÍN,[2] VICTORIA MASAGUER.[3]

[1.] Instituto Nacional del Carbón, INCAR-CSIC, Apartado 73, 33080 Oviedo, Spain;

[2.] LEQUIA, Universitat de Girona, Campus de Montilivi s/n, 17071 Girona, Spain;

[3.] ArcelorMittal Global R&D Asturias, CDT, Apartado 90, 33400 Avilés, Spain.

Corresponding author phone: +34 985118996; fax: +34 985299076; e-mail: miguel.montes@csic.es

Abstract

Slags collected from the basic oxygen furnaces of two Linz-Donawitz steel making plants were tested as adsorbents for H_2S removal at room temperature (298 K). Two different particle size fractions, namely < 212 and 212-500 μm, were selected from the original slag samples. Dynamic adsorption tests were carried out using a column-bed configuration and retention capacities were calculated after bed exhaustion. Retention capacities as high as 180 mg of H_2S g^{-1} of slag were attained, in spite of the very low specific surface area of the steel slags. As expected, humidity played a crucial role in the removal of H_2S. Particle size had also an important effect on the capacity of the adsorption beds. Analysis of the exhausted slags revealed considerable amounts of elemental sulfur on the surface of the particles. Sulfates were also found on the exhausted slags, especially on the 212-500 μm size fractions. The characterization of the slags prior and after the H_2S adsorption experiments allowed us to postulate plausible mechanisms to understand the outstanding capacity of these steel by-products for H_2S adsorption.

Introduction

The integrated production of steel comprises the generation of significant amounts of by-products and wastes. LD (after Linz and Donawitz) slag originates during the transformation of molten pig iron produced in a blast furnace into liquid steel. The LD process is carried out in an oxidising atmosphere to reduce the carbon content of the pig iron to adequate levels. In terms of quantities, LD slag (aka Basic Oxygen Furnace or BOF slag) ranks second (1-4), with typical production percentages fluctuating around 10-20% by weight of steel outputs.

The composition of the LD steel slags limits to some extent their re-use within the integrated process. For instance, residual amounts (> 0.05 wt.%) of phosphorous and sulfur make the slag unfeasible to replace raw materials (limestone, iron ore) in the blast furnace, whereas recycling through the sinter plant is also limited by phosphorous, alumina and titanium contents (1,5). Other uses in the steel plants are mostly constrained by costs and nowadays in-situ valorisation of the slag seems restricted to the magnetic recovery of metals. Therefore, there is a continuous search for markets that could eventually absorb the massive amounts of LD slags produced per year. Civil construction has been already spotted and LD slags are currently employed as sub-bases in roads. However, materials for civil engineering must comply with tight specifications in terms of hydraulic expansion, which most LD slags find difficult to fulfil, due to their significant CaO, MgO and metallic Fe contents (6).

This situation has prompted an increasing interest in alternative routes of LD slag valorisation. Among them, their use as low-cost adsorbents of pollutants in gaseous effluents (7-9), and wastewater (10-12) has been widely investigated. Although these alternatives may seem rather limited in terms of the amounts of slag eventually re-used, they have caught the attention of steel companies. Indeed, replacing conventional adsorbents for steel by-products in the treatment of the effluents

generated within the steel integrated process sounds most advantageous from both environmental and economic viewpoints.

On the other hand, diffuse H_2S emissions are common in coking plants despite the coke oven gas desulfurization technologies in integrated steel plants (13-15). Stringent environmental policies compel companies to mitigate those emissions down to very low levels, the situation becoming especially acute for steel plants located near residential areas. In this regard, the use of solid adsorbents/catalysts such as activated carbons (ACs) (16-18), or mixed oxides (19,20) has been proven a competitive technology for H_2S removal at low temperatures, despite the high operational costs, mainly related to the price of the adsorbent/catalyst.

This work is part of a project steered by ArcelorMittal to explore different alternatives of LD slag valorisation. LD steel slags are proposed herein as suitable candidates to replace conventional adsorbents/catalysts for removing H_2S at room temperature on the basis of their chemical nature. The combination of metal (mainly iron) oxides with the strong alkalinity could make the surface of this by-product an adequate environment for the retention of H_2S from gaseous streams.

Experimental Section

Representative samples (10 kg) of “as produced” LD steel slags (size class 0-10 mm) were collected in the two ArcelorMittal plants located in Asturias (NW of Spain), namely ArcelorMittal Avilés (sample SA) and ArcelorMittal Veriña (sample SV). Sampling was carried out by qualified plant personnel with a shovel-like tool. The elemental composition of the slags was then checked to lie within the ranges established by the company to consider the slag sample as representative of a given plant. In the case of SV, a milling process has been implemented in the slag treatment plant to favour metal recovery; as a consequence, all the LD slag produced in the Veriña plant is size class 0-10 mm. As received samples were sieved in the laboratory and the different size

fractions stored in appropriate containers to minimise aging. Only two size fractions (<212 and 212-500 μm) were considered for the H_2S adsorption experiments (see Results and Discussion).

Dynamic H_2S removal experiments were carried out in a fixed bed configuration, at room temperature (298 ± 2 K). The H_2S inlet concentration was set to 1000 ppmv (parts per million by volume) in moist air. About 0.5 g of the slag were placed inside a quartz reactor (7 mm i.d.), ensuring uniform flow (150 ml min^{-1}) of moist air throughout the bed and avoiding axial dispersion. Typical bed heights ranged between 8-10 mm. Independent experiments were carried out with air moistened at two different relative humidity (R.H.) values, 10% and 50%, to assess the effect of this parameter on the final performance of the adsorption beds. Inlet and outlet H_2S concentrations (c_{in} and c_{out}, respectively) were monitored using a μGC (Varian CP-4900) equipped with a thermal conductivity detector (TCD). The gas chromatograph was fitted with a 10 m PPQ column unit. Helium was employed as carrier gas. The injector temperature was set at 383 K; the oven temperature and inlet pressure were hold constant at 318 K and 1.5 10^5 Pa, respectively. Adsorption capacities (x/M, mg H_2S g^{-1} slag) were calculated by integration of the breakthrough curves as reported elsewhere (21). At least three adsorption experiments were performed for each size fraction and R.H. value in order to attain statistical soundness.

Fresh and exhausted slags were characterized by different techniques. Details of the experimental procedures and apparatus are included in the Supporting Information (SI).

Results and discussion

In order to avoid the processing costs involved in an eventual milling of the slag, as-received LD samples were sieved and selected fractions were considered for carrying out the H_2S removal experiments. Figure 1 shows the particle size distribution

of the SA and SV original samples. The lower proportion of fine particles in SV slag compared to SA is attributed to the magnetic metal recovery process used in the plant in Veriña, which seems very effective in removing small (ferromagnetic) particles. Although the distributions shown in Figure 1 should be considered representative of the slag produced in the selected factories, variations of the particle size distribution may be expected from batch-to batch due to changes in the cooling conditions of the LD slag (22). Nevertheless, only the two smallest size fractions, which account for almost 20 % and 10 % by weight of the SA and SV slags, respectively, will be herein investigated.

The elemental composition (major constituents) of the two LD slag size fractions selected, as measured by XRF, is presented in Table 1. Differences in iron and, in the case of SV, magnesium contents of the fractions under consideration with respect to the original samples (see experimental section) are significant. The low Fe content in the smallest fractions may be related to the relative hardness of the metallic particles that would be more difficult to disaggregate by attrition. The lower percentages of iron species in the two studied fractions are balanced with the large increase of the loss on ignition values, when compared to the analyses of the original size class (i.e, 0-10 mm). This latter observation can be explained in terms of the higher surface to volume ratios of the fine particles, which should favour natural carbonation and hydration processes. Figure 2 shows the TGA profiles obtained for different size fractions of the SV slag. The main weight losses centred at about 720 K and 990 K, corresponding to the de-hydration of $Ca(OH)_2$ and decomposition of $CaCO_3$, respectively, decrease as the mean particle size of the sample tested increases.

Comparison of the TG profiles of the SV < 212 fraction under air and nitrogen reveals an additional contribution to the loss on ignition at temperatures above 1000 K (accounting for ca. 1-2 wt.%). This has been observed for slag fractions below 500 μm and has been related to the presence of highly pure carbon particles. A SEM

micrograph of these particles is shown in Figure 2 (inset). Indeed, EDX analysis confirmed that it such grey areas are mainly composed of pure carbon. The geometry and lamellar structure of these carbon particles suggest they could be graphite flakes; the intense reflection peak at 26.5º 2θ (Figure 2, inset; Figure SI1) in the XRD patterns of the LD slags also confirmed this hypothesis. The presence of graphite flakes seems most plausible since carbon is prone to be formed in specific areas of the LD steel plant where a very rich CO gas atmosphere eventually reaches temperatures well above 1300 K, thus displacing de Boudouard equilibrium towards the formation of pure C and CO_2 (24). It is worth pointing out that similar XRD reflections in steelmaking slags have been traditionally assigned to crystalline SiO_2 (23).

Assignments of the different reflections observed in the XRD patterns of the slags were very uncertain due to the strong background and the diversity of plausible crystalline species that may be present, thus causing the overlap of peaks. Only three other crystalline phases were identified as portlandite, calcite, and lime (Figure SI1) in all the samples, whereas magnesium compounds (periclase and brucite) were also observed in the SV fractions.

Dynamic H_2S adsorption experiments were carried out until bed exhaustion. Moist air at two R.H. values was circulated through the bed in independent tests to assess the effect of moisture on the final performance of the LD slags. Examples of the breakthrough curves obtained for the four samples studied are shown in Figure SI2. All breakthrough curves are very neat and quite symmetrical. H_2S retention capacities (x/M) have been calculated and average values are plotted in Figure 3. As expected from pervious results obtained with different types of adsorbents/catalysts (16,25,26), humidity strongly favours the retention of H_2S on the slags. x/M values of almost 20 wt.% are attained for SV 212-500 when the adsorption column operated at ca. 50 % R.H. This is an outstanding result considering the low pore volumes of the sample ($V_t \leq 0.05$ cm^3 g^{-1}, see Figure SI3). The retention capacity of the slags

compares reasonably well with that reported for low-cost adsorbents prepared from residues (21), but is far behind the values obtained for tailored ACs (ranging between 300-600 mg H_2S/ solid mass) (16). When the moisture of the inlet flow lowers down to 10 % R.H., all samples perform similarly showing a drop in the x/M value to around 30 mg H_2S / g slag (Figure 3). It must be reminded here that the adsorption beds were pre-humidified prior to experiments. As observed for other materials (27), wetting of the slags particles before testing changes dramatically their capacity for H_2S removal -almost negligible uptake is observed for non pre-humidified beds-. The effect of R.H. on x/M values (Figure 3) would then indicate that relatively high inlet moisture is required to prevent a substantial drying of the bed. Henceforth, only those results obtained for tests carried out at 50 % R.H. will be further discussed.

Direct observation of the beds after the dynamic adsorption experiments revealed the presence of elemental S on the exhausted samples (yellowish colour). Further characterization by SEM/EDX analysis showed that sulfur clusters practically cover the surface of the exhausted slag particles (Figure SI4). Crystal aggregates became especially noticeable at the brighter spots of the EDX signal of Figure SI4; sulphur crystalline structures were further confirmed by XRD (Figure SI5). Elemental sulfur is also responsible for the weight loss observed in the N_2 TG profiles of the exhausted samples between 430-550 K (Figure 5).

The complex chemical composition of LD slags makes rather challenging to elucidate a plausible mechanism to explain their superior performance for H_2S uptake. Results in Figure 3 pinpoint the chemical reactions occurring in aqueous solution (i.e., the water layer over the solid particles) and the slags basic character as key factors. The strong basicity of the slags would trigger the dissociation of dissolved H_2S into S^{2-} and HS^- anions. Further reactions would involve anion exchange with OH^- or even O^{2-} not only in the homogeneous (aqueous) phase but also on the outermost solid surfaces. Subsequently, redox and/or precipitation reactions would follow to bring about the final

products. Thus, a feasible mechanism to explain the H_2S removal capacity of these steel residues would be based on a redox process in which transition metals oxides and/or hydroxides should act as active catalysts for the oxidation of hydrogen sulfide to elemental sulfur. More specifically, Fe (III) hydrated oxides (or hydroxides) have been long used in the desulfurisation of coke oven gas (28,29). In strong alkaline medium (i.e., in the presence of slags), the following reactions are favoured (30):

$$2Fe(OH)_3 + 3H_2S \rightarrow 2FeS + 1/8S_8 + 6H_2O \quad (1)$$

$$4FeS + 3O_2 \rightarrow 2Fe_2O_3 + 1/2S_8 \quad (2)$$

These two reactions should account for most of the elemental sulfur detected in the exhausted slags, which, as estimated from the TG analysis (Figure 5), amounts for around 75 mg S/g dry fresh slag, regardless the particle size fraction or origin of the slag. This value is slightly above the theoretical maximum of 60 mg H_2S /g Fe_2O_3 established in the literature (30), according to the iron contents of the slags (Table 2). To understand this apparent misleading result the following aspects must also be pondered: i) other transition metal oxides, such as MnO, might also contribute to the formation of elemental sulfur in a similar fashion to that of iron oxides; and ii) reaction of hydrogen sulfide with iron oxides (or hydroxides) does not only render elemental sulfur (see below).

An additional thermal event between 1000-1250 K appears for the exhausted samples, which is not observed for the fresh samples (Figure 5). To identify this peak, the exhausted samples were also investigated by means of thermogravimetric analysis coupled to mass spectrometry (TG-MS), recording several m/z fragments of the evolved gases (i.e., m/z 32, 44 and 64). The thermal event above 1000 K observed in the TG profiles (Figure 5) matched to the m/z = 64 signal in Figure 6, evidencing the evolution of SO2 likely arising from the decomposition of sulfates. Based on the chemical composition of the slags, the source of sulfates accounting for the DTG peak at ca. 1125 K (Figures 5 and 6) seems somewhat unclear. However, small amounts of

sulfates (and thiosulfates) are reported to be formed during the desulfurisation of gases with iron oxides when oxygen is present in the carrier gas (20):

$$2Fe(OH)_3 + 3H_2S + 6O_2 \rightarrow Fe_2(SO_4)_3 + 6H_2O \quad (3)$$

$$2Fe(OH)_3 + 2H_2S + 7/2O_2 \rightarrow 2FeSO_4 + 5H_2O \quad (4)$$

However, iron sulfates decompose at temperatures well below 1000 K, the threshold temperature assigned to the decomposition of sulfates in the exhausted slags (Figures 5 and 6). Although the presence of $MnSO_4$ cannot be discarded (initial decomposition temperature of 980 K), we reckon that, in spite of its relatively high temperature of decomposition (around 1450 K), $CaSO_4$ seems the most plausible sulfate present in the surface of the exhausted slags, hence accounting for the DTG peak at 1125 K. This hypothesis seems reasonable if the abundance of calcium species on the moist surface of the slag particles and the low solubility of $CaSO_4$ (compared to iron sulfates) are taken into consideration. To further demonstrate this hypothesis, an aliquot of the exhausted samples was heated up to 573 K under inert atmosphere to wipe off the elemental sulfur deposits described above, hence facilitating the identification of other sulfur species. SEM/EDX analysis of those thermally treated, exhausted samples revealed the presence of clusters of needle-like crystals (Figure SI6) with a composition resembling that of calcium sulphate. Furthermore, the presence of reducing agents such as graphite in the vicinity of $CaSO_4$ grains should explain the drop of its decomposition temperature down to that observed in Figure 6 (31), likely following the equation:

$$2CaSO_4 + C \rightarrow CaS + CaO + SO_2 + 3/2O_2 + CO_2 \quad (5)$$

TG-MS studies confirmed the evolution of O_2 (m/z = 32) and CO_2 (m/z = 44) between 1000-1200 K (Figure 6). Other moieties such as SiO_2, silicates and even metal sulfides are also known to lower the temperature of decomposition of the $CaSO_4$ (31). The evolution of O_2 and CO_2 was also observed between 600-720 K (to a much lower

extent) and has been ascribed to the decomposition of very small amounts of $Fe_2(SO_4)_3$ or $FeSO_4$ remaining on the slag particles. A reaction similar to that postulated in equation 5 could also apply for the reduction in the decomposition temperature of iron sulfates in the presence of reducing agents.

The formation of sulfides after H_2S adsorption on the slags was a priori also expected as predicted from equation 1. In addition, a route for the formation of FeS_2 has been suggested through the oxidation of FeS (20):

$$3FeS + 1/2O_2 + H_2S \rightarrow FeS_2 + H_2O \qquad (6)$$

In this work, however, no evidences could be gathered supporting the presence of significant amounts of sulfides on the exhausted slags. Sulfides could not be detected in TG experiments since they melt, rather than decompose, during the thermal treatment. Additionally, XPS analysis of exhausted samples treated at 573 K under non oxidising conditions (to remove elemental sulfur) was also performed (Figure SI7a). XPS data of the S2p peak revealed a well-defined band centered at ca. 171 eV (binding energy), which suggests that only sulfates would cover the outer surface of the slag particles (Figure SI7b).

In fact, S^{2-} species were only identified on the exhausted samples after thermal treatment at high temperatures (> 973 K) under non-oxidising conditions by XRD and SEM/EDX analyses. The XRD patterns of the exhausted slags treated at 995 K (Figure SI8) showed some reflections assigned to iron sulfides (also spotted by SEM/EDX), whereas CaS was detected after treatment of the exhausted slags above 1300 K (Figure SI9). The detection of sulfides seems to be related to sulfates decomposition assisted by reducing agents (equation 5) rather than to the formation of sulfides during the H_2S removal experiments. Indeed, the precipitation of highly insoluble FeS might be hampered by the strong alkalinity of the medium (32). On the other hand, precipitation of CaS might be limited by the sensitivity of calcium sulfide to water and oxygen environments (33).

A quantitative sulfur balance was carried out in terms of the amount of sulfur (expressed on a dry fresh slag basis) calculated from the weight loss assigned to elemental sulfur (Figure 5) and the overall H_2S adsorption capacity of the slags calculated from the x/M data plotted in Figure 3. For example, of the 109 mg of sulfur adsorbed (as H_2S) per gram of dry sample SV< 212, ca. 73 mg correspond to elemental S. Calculations for the studied samples are shown in Figure 7, and the obtained data indicate that the amount of H_2S converted to elemental sulfur is very similar for all slags tested. The amount of sulfur to complete the bar (i.e., 36 mg for SV< 212) is tentatively assigned to the presence of sulfates in the exhausted sample. As a consequence, the formation of sulfates during the H_2S adsorption tests seems determinant for the higher retention capacities of the 212-500 μm size fractions. XPS results support this hypothesis, i.e., more than twice atomic concentration of sulfur (as sulfates) remains on the surface of the 212-500 μm size fractions saturated with H_2S plus thermally treated (573 K) when compared to the < 212 μm ones (Figure SI7a). In terms of chemical composition, a possible explanation for this observation is the higher amounts of oxidized Fe -i.e., Fe(II)+Fe(III)- found in the 212-500 μm size fractions (Table 2). Also, the superior performance of these fractions may be related to engineering parameters such as the permeability of the adsorption bed. Further work is currently under progress at a pilot plant scale in which slags with higher particle size fractions are being tested.

Acknowledgments

This work was partially funded by the PCTI-Asturias (Projects PEST08-07, PEST08-14 and PC10-71).

Supporting Information Available

Details of the slags characterization methodologies, as well as several figures cited in the text are provided as Supporting Information in a separate file. This information is available free of charge via the Intertnet at http://pubs.acs.org/.

Brief

LD steel-slags can remove a 20% by weight of H_2S from moist air, at room temperature.

Literature Cited

(1) Das, B.; Prakash, S., Reddy, P. S. R.; Misra, V. N. An overview of utilization of slag and sludge from steel industries. *Resour. Conserv. Recy.* **2007,** *50,* 40-57.

(2) Proctor, D.M.; Fehling, K. A.; Shay, E. C.; Wittenborn, J. L.; Green, J. J.; Avent, C.; Bigham, R. D. Physical and chemical characteristics of blast furnace, basic oxygen furnace, and electric arc furnace steel industry slags. *Environ. Sci. Technol.* **2000,** *34,* 1576-1582.

(3) Ficha técnica de escorias de acería. CEDEX (2007). http://www.cedexmateriales.vsf.es/view/archivos/residuos/282.pdf

(4) Reddy, A. S.; Pradhan, R. K.; Chandra, S. Utilization of Basic Oxygen Furnace (BOF) slag in the production of a hydraulic cement binder. *Int. J. Miner. Process.* **2006,** *79,* 98-105.

(5) Chaurand, P.; Rose, J.; Domas, J.; Bottero, J-Y. Speciation of Cr and V within BOF steel slag reused in road constructions. *J. Geochem. Explor.* **2006,** *88,* 10-14.

(6) Shen, W.; Zhou, M.; Ma, W.; Hu, J.; Cai, Z. Investigation on the application of steel slag-fly ash-phosphogypsum solidified material as road base material. *J. Hazard. Mater.* **2009,** *164,* 99-104.

(7) Huijgen, W. J. J., Witkamp, G-J.; Comans, R. N. J. Mineral CO_2 sequestration by steel slag carbonation. *Environ. Sci. Technol.* **2005,** *39,* 9676-9682.

(8) Huijgen, W. J. J.; Comans, R. N. J. Carbonation of steel slag for CO_2 sequestration: Leaching of products and reaction mechanisms. *Environ. Sci. Technol.* **2006,** *40,* 2790-2796.

(9) Bonenfant, D.; Kharoune, L.; Sauvé, S.; Hausler, R.; Niquette, P.; Mimeault, M.; Kharoune, M. CO_2 sequestration potential of steel slags at ambient pressure and temperature. *Ind. Eng. Chem. Res.* **2008,** *47,* 7610-7616.

(10) Bowden, L. I.; Jarvis, A. P.; Younger, P. L.; Johnson, K. L. Phosphorous removal from waste waters using basic oxygen steel slag. *Environ. Sci. Technol.* **2009,** *43,* 2476-2481.

(11) Aguirre, N. V.; Vivas, B. P.; Montes-Morán, M. A.; Ania, C. O. Adsorption of thiocyanate anions from aqueous solutions onto adsorbents of various origin. *Ads. Sci. Technol.* **2010,** *28,* 705-716.

(12) Cha, W.; Kim, J.; Choi, H. Evaluation of steel slag for organic and inorganic removals in soil aquifer treatment. *Water Res.* **2006,** *40,* 1034-1042.

(13) Diemer, P.; Killick, H-J.; Knop, K.; Lüngen, H. B.; Reinke, M.; Schmöle, P. Potentials for utilisation of coke oven gas in integrated iron and steel works. *Stahl and Eisen Comm.* **2004,** *124,* 21-30.

(14) UK Environmental Agency. 2004. Integrated Pollution Prevention and Control (IPPC). S2.01: Guidance for the Production of Coke, Iron and Steel. Issue 1: June 2004. Bristol: Environment Agency.

(15) European Commission. 2011. European Integrated Pollution Prevention and Control Bureau (EIPPCB). Best Available Techniques (BAT) reference document for Iron and Steel Production. Industrial Emissions Directive 2010/75/EU. Draft Version (June 2011).

(16) Bandosz, T. J. On the adsorption/oxidation of hydrogen sulfide on activated carbons at ambient temperatures. *J. Colloid Interface Sci.* **2002**, *246*, 1-20.

(17) Yan, R.; Liang, D. T.; Tsen, L.; Tay, J. H. Kinetics and mechanisms of H_2S adsorption by alkaline activated carbon. *Environ. Sci. Technol.* **2002**, *36*, 4460-4466.

(18) Klein, J.; Henning, K-D. Catalytic oxidation of hydrogen sulphide on activated carbons. *Fuel* **1984**, *63*, 1064-1067

(19) Baird, T.; Campbell, K. C.; Holliman, P. J.; Hoyle, R.; Noble, G.; Stirling, D.; Williams, B. P. Mixed cobalt-iron oxide absorbents for low-temperature gas desulfurisation. *J. Mater. Chem.* **2003**, *13*, 2341-2347.

(20) Cantrell, K. J.; Yabusaki, S. B.; Engelhard, M. H.; Mitroshkov, A. V.; Thorntorn, E. C. Oxidation of H_2S by iron oxides in unsaturated conditions. *Environ. Sci. Technol.* **2003**, *37*, 2192-2199.

(21) Ros, A.; Lillo-Ródenas, M. A.; Canals-Batlle, C.; Fuente, E.; Montes-Morán, M. A.; Martin, M. J.; Linares-Solano, A. A new generation of sludge-based adsorbents for H_2S abatement at room temperature. *Environ. Sci. Technol.* **2007**, *41*, 4375-4381.

(22) Tossavainen, M.; Engstrom, F.; Yang, Q.; Menad, N.; Larsson, M. L.; Bjorkman, B. Characteristics of steel slag under different cooling conditions. *Waste Manag.* **2007,** *27,* 1335-1344.

(23) Navarro, C.; Díaz, M; Villa-García, M. A. Physico-chemical characterization of steel slag. Study of its behavior under simulated environmental conditions. *Environ. Sci. Technol.* **2010**, *44*, 5383-5388.

(24) *An Introduction to Iron and Steel Processing.* JFE 21st Century Foundation (2003). http://www.jfe-21st-cf.or.jp/chapter_2/index.html

(25) Bagreev, A; Bandosz, T. J. On the mechanism of hydrogen sulfide removal from moist air on catalytic carbonaceous adsorbents. *Ind. Eng. Chem. Res.* **2005,** *44,* 530-538.

(26) Ros, A.; Montes-Morán, M. A.; Fuente, E.; Nevskaia, D. M.; Martin, M. J. Dried sludges and sludge-based chars for H_2S removal at low temperature: Influence of sewage sludge characteristics. *Environ. Sci. Technol.* **2006**, *40*, 302-309.

(27) Bagreev, A; Bandosz, T. J. H_2S adsorption/oxidation on unmodified activated carbons: Importance of prehumidification. *Carbon* **2001,** *39,* 2303-2311.

(28) Więckowska, J. Catalytic and adsorptive desulphurization of gases. *Catal. Today* **1995,** *24,* 405-465.

(29) Miura, K., Mae, K., Inoue, T., Yoshimi, T., Nakagawa, H., Hashimoto, K. Simultaneous removal of COS and H_2S from coke oven gas at low temperature by use of an iron oxide. *Ind. Eng. Chem. Res.* **1992,** *31,* 415-419.

(30) Davydov, A.; Chuang, K. T.; Sanger, A. R. Mechanism of H_2S oxidation by ferric oxide and hydroxide surfaces. *J. Phys. Chem.* **1998,** *102,* 4745-4752.

(31) Hull, W. Q.; Schon, F.; Zirngibl, H. Sulfuric acid from anhydrite. *Ind. Eng. Chem.* **1957,** *49,* 1204-1214.

(32) Rickard, D.; Luther III, G. W. Chemistry of iron sulfides. *Chem. Rev.* **2007,** *107,* 514-562.

(33) Roy, A. Sulfur speciation in granulated blast furnace slag: An X-ray absorption spectroscopic investigation. *Cement Concrete Res.* **2009,** *39,* 659-663.

Table 1. Elemental composition of the LD slags determined in different size fraction samples.

Sample	Elemental composition (% db[a])									
	SiO_2	Al_2O_3	Fe_2O_3	CaO	MgO	MnO	TiO_2	P_2O_5	S^d	LOI[b]
SA < 212	11.6	2.8	18.4	42.7	5.1	3.0	0.4	1.1	0.1	14.1
SA 212-500	12.9	3.0	21.6	42.4	4.6	3.5	0.5	1.1	0.1	9.4
SA (0-10)[c]	14.1	2.5	28.7	47.0	4.5	4.2	0.5	1.3	0.2	2.6
SV < 212	12.7	3.7	16.8	35.4	14.0	2.4	0.4	0.7	0.1	13.2
SV 212-500	12.9	3.9	22.4	37.1	8.7	2.9	0.4	0.8	0.1	12.0
SV (0-10)[c]	16.5	2.5	33.4	43.8	5.6	4.2	0.5	1.3	0.2	-0.1

(a) Dry basis
(b) Loss on ignition (at 1223 K)
(c) Original samples (from which <212 and 212-500 size fractions were obtained)
(d) Sulfur content, as determined by elemental analysis

Table 2. Results of the iron speciation of the LD slag samples under consideration.

Sample	Elemental composition (% db[a])				
	Fe total	Fe(II)	Fe(0)	Fe(III)	Fe(II)+Fe(III)
SA < 212	12.9	4.0	3.1	5.8	9.8
SA 212-500	15.1	7.4	1.7	6.0	13.4
SV < 212	11.7	2.4	2.6	6.7	9.1
SV 212-500	15.7	4.0	4.0	7.7	11.6

(a) Dry basis

Figure Captions

Figure 1. Particle size distribution of the SA (0-10) and SV (0-10) original slag samples.

Figure 2. TG experiments of different slag fractions under oxidising and non-oxidising atmosphere. SV 3-4 stands for the 3-4 mm fraction of SV slag (see Figure 1). Inset: SEM micrograph of SV< 212 showing a graphite particle. Inset: XRD pattern of SV< 212 showing a very strong reflection at 26.5 º ascribed to the presence of graphite.

Figure 3. H_2S retention capacities of the slags under consideration obtained in experiments carried out at two different relative humidity (R.H.) values.

Figure 4. SEM micrograph showing elemental S crystals on a SA< 212 exhausted sample.

Figure 5. TG and DTG profiles (under nitrogen) of SA< 212 samples before and after the H_2S removal tests.

Figure 6. Simultaneous DTG profile (under nitrogen) and evolution of different mass spectral lines with temperature of SV< 212 exhausted sample.

Figure 7. Semi-quantitative sulfur balance of the exhausted slag samples.

FIGURE 1

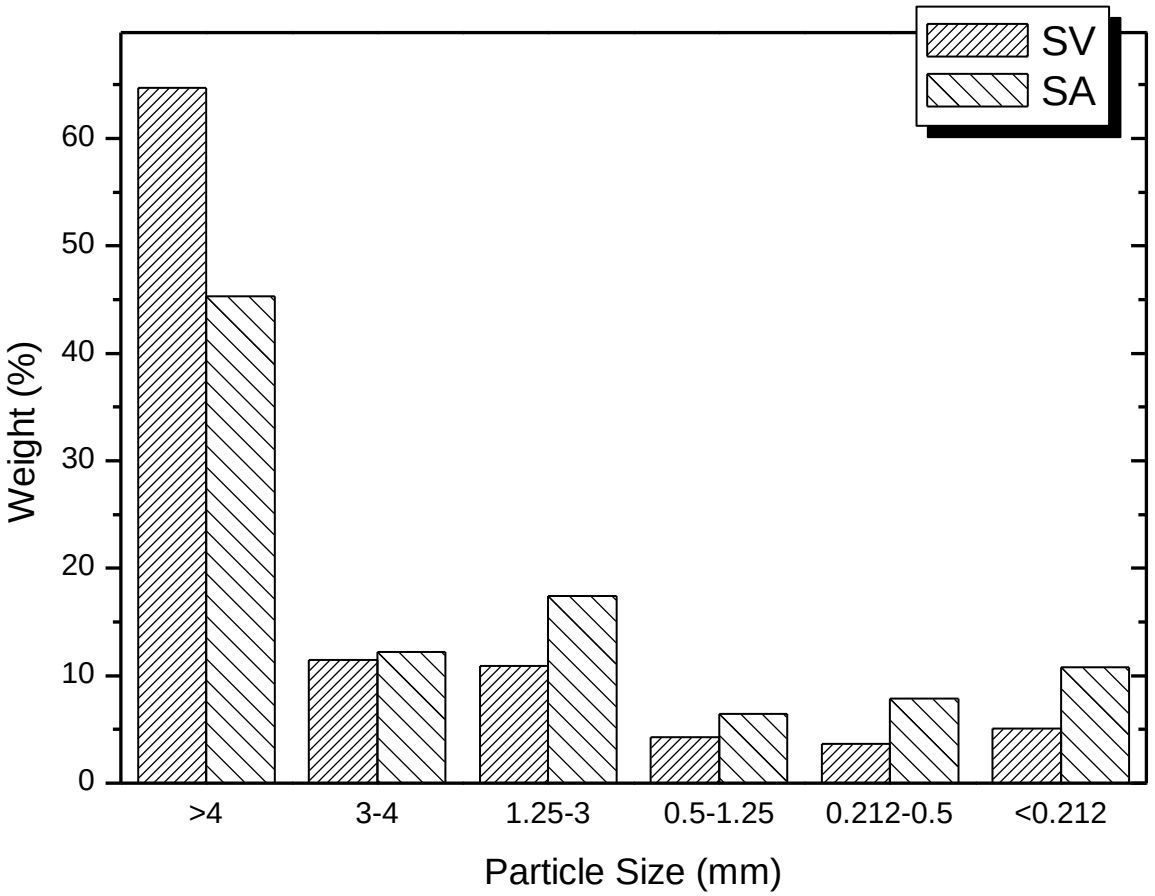
SV
SA
Weight (%)
0
10
20
30
40
50
60
>4
3-4
1.25-3
0.5-1.25
0.212-0.5
<0.212
Particle Size (mm)

FIGURE 2

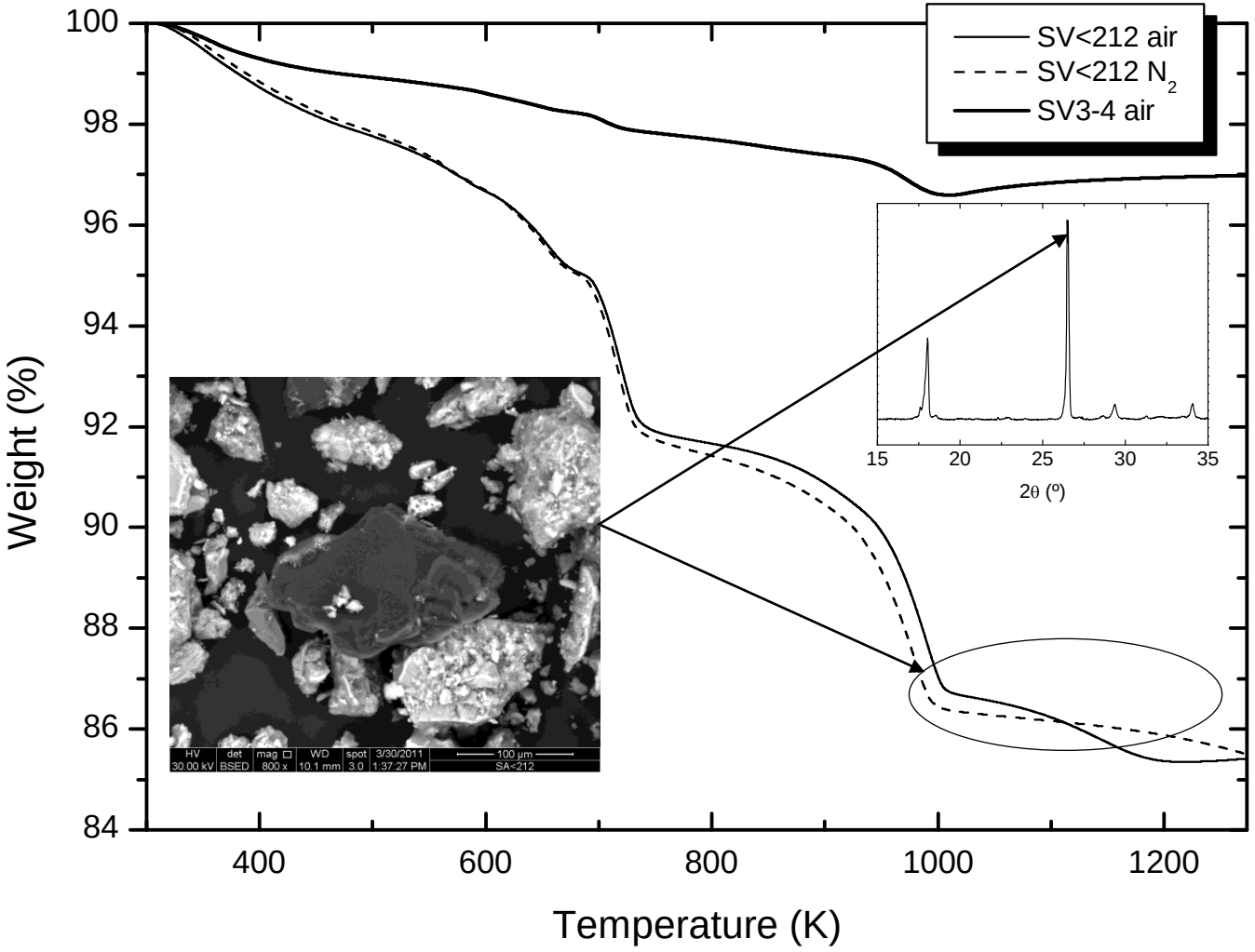
SV<212 air
SV<212 N2
SV3-4 air
Weight (%)
Temperature (K)
100
98
96
94
92
90
88
86
84
400
600
800
1000
1200
15
20
25
30
35
2θ (º)
HV
30.00 kV
det
BSED
mag
800 x
WD
10.1 mm
spot
3.0
3/30/2011
1:37:27 PM
100 µm
SA<212

FIGURE 3

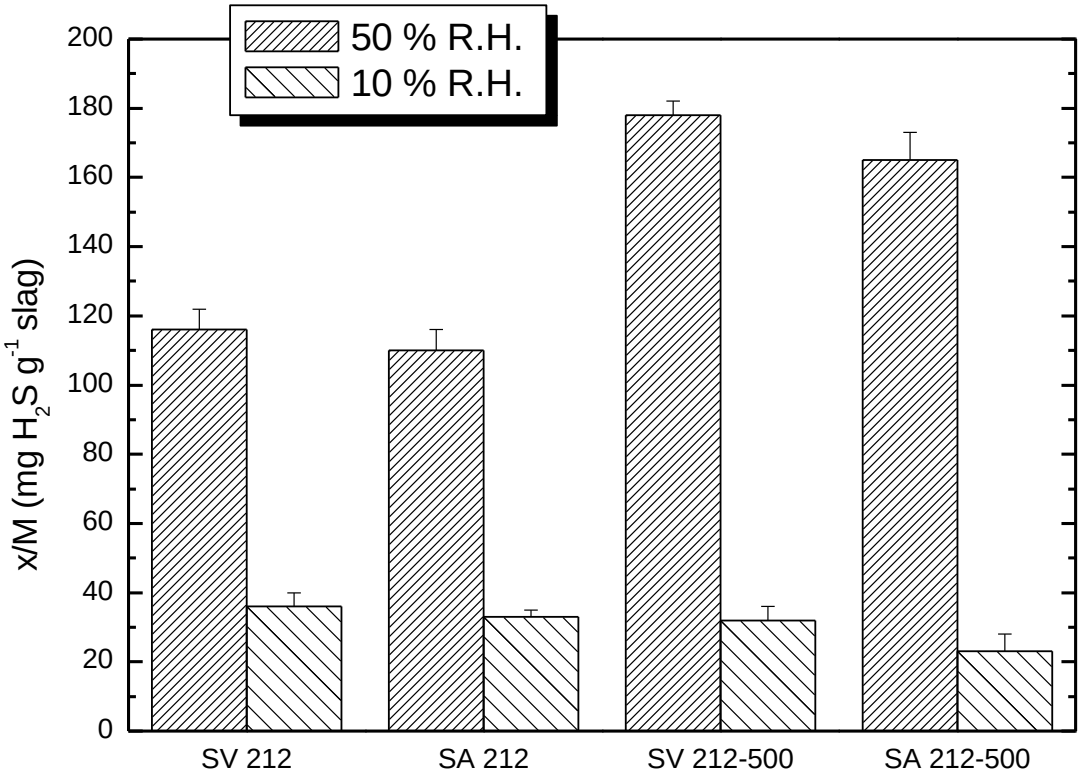
50 % R.H.
10 % R.H.
x/M (mg H_2S g^{-1} slag)
0
20
40
60
80
100
120
140
160
180
200
SV 212
SA 212
SV 212-500
SA 212-500

FIGURE 4

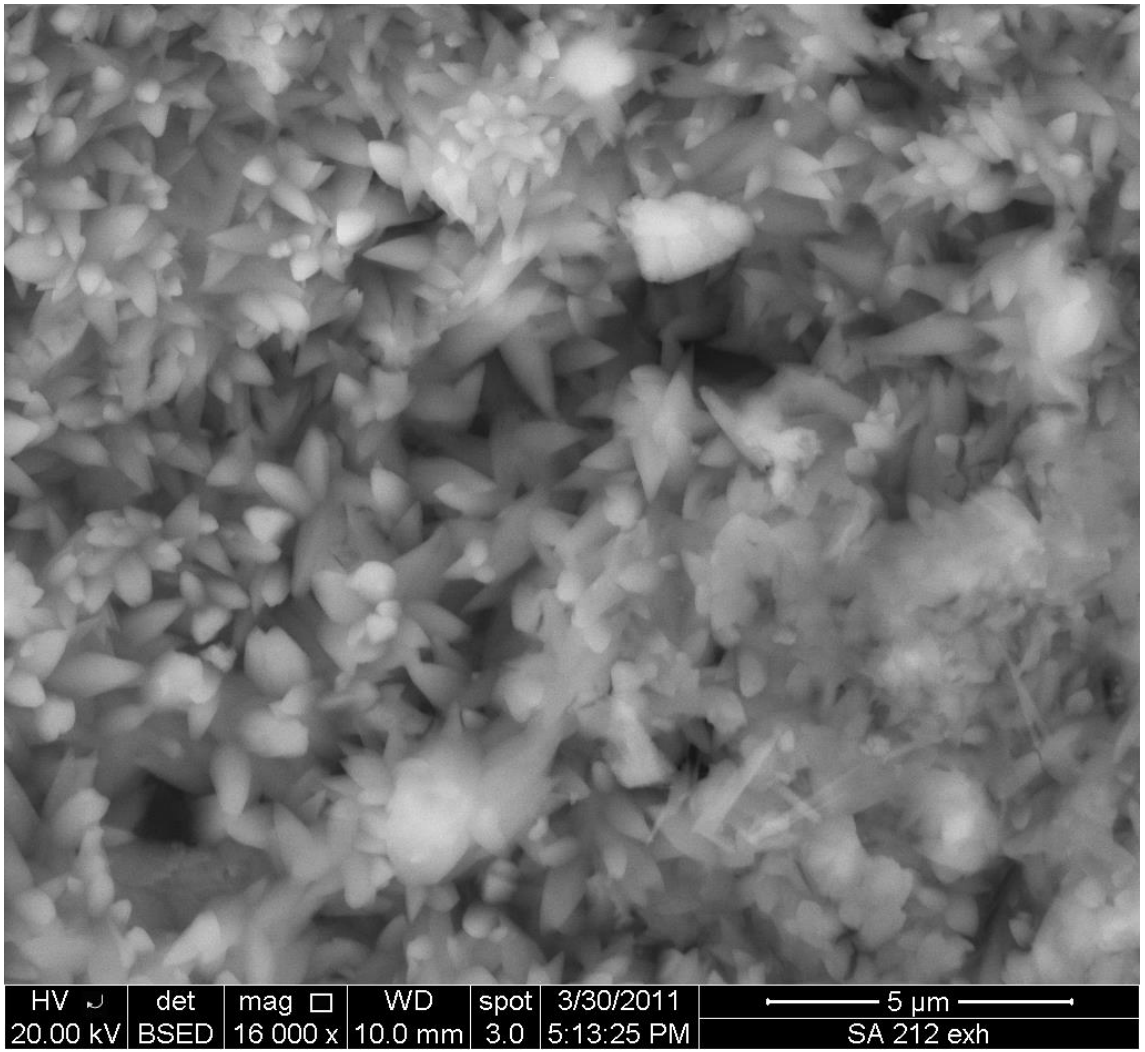
HV
20.00 kV
det
BSED
mag
16 000 x
WD
10.0 mm
spot
3.0
3/30/2011
5:13:25 PM
5 µm
SA 212 exh

FIGURE 5

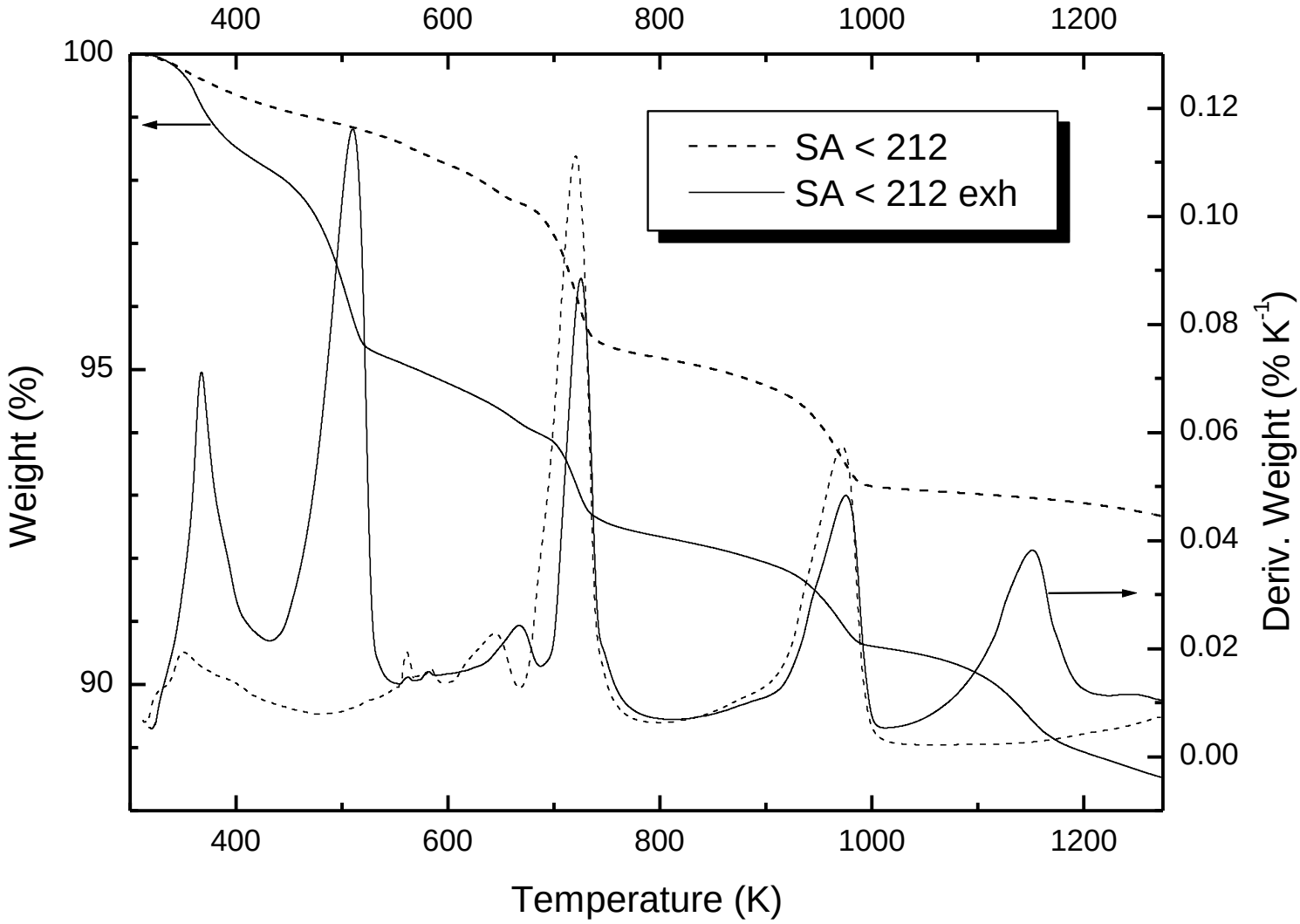
400
600
800
1000
1200
100
95
90
Weight (%)
SA < 212
SA < 212 exh
0.12
0.10
0.08
0.06
0.04
0.02
0.00
Deriv. Weight (% K-1)
Temperature (K)

FIGURE 6

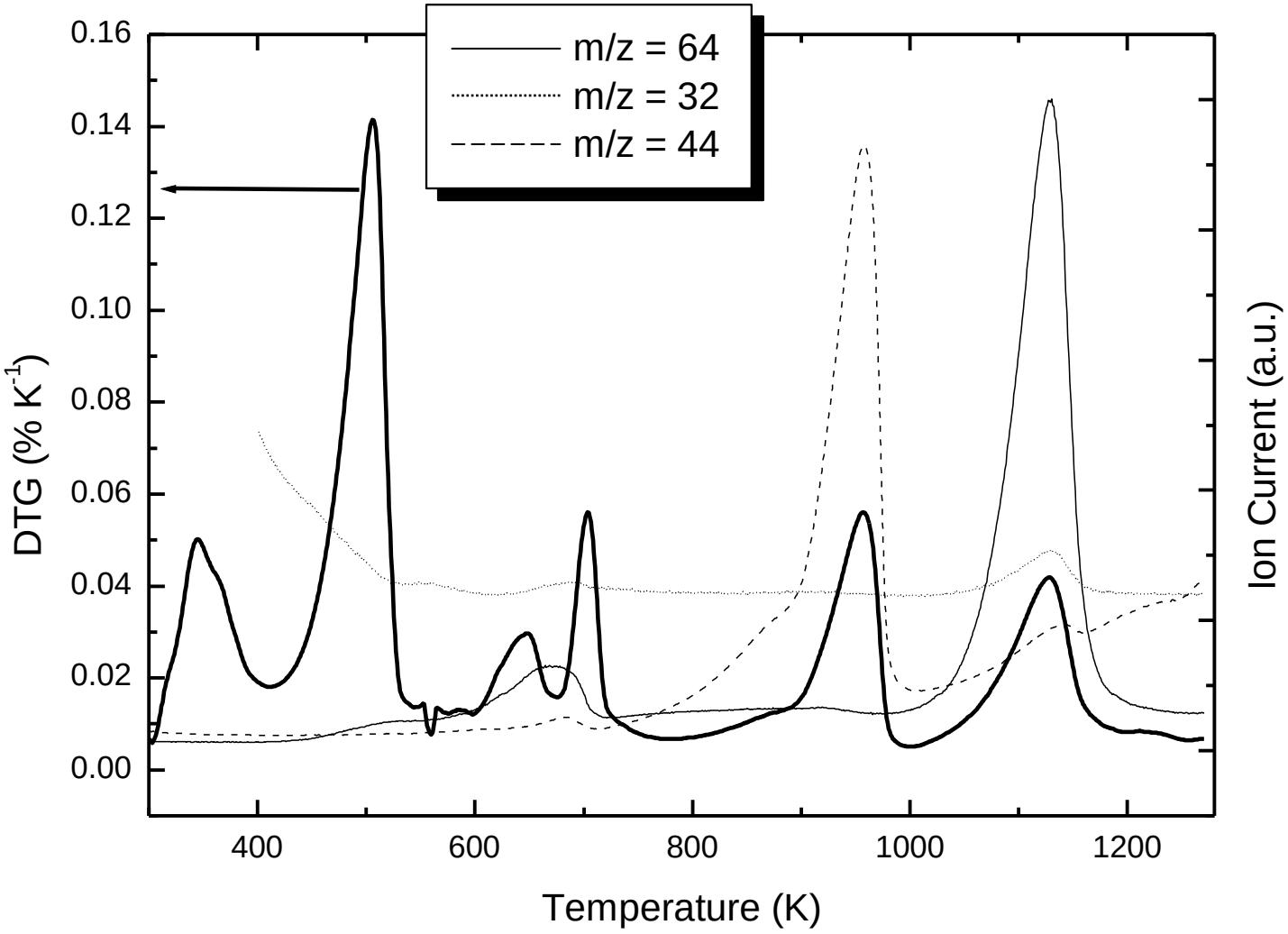
m/z = 64
m/z = 32
m/z = 44
DTG (% K-1)
Ion Current (a.u.)
Temperature (K)
0.16
0.14
0.12
0.10
0.08
0.06
0.04
0.02
0.00
400
600
800
1000
1200

FIGURE 7

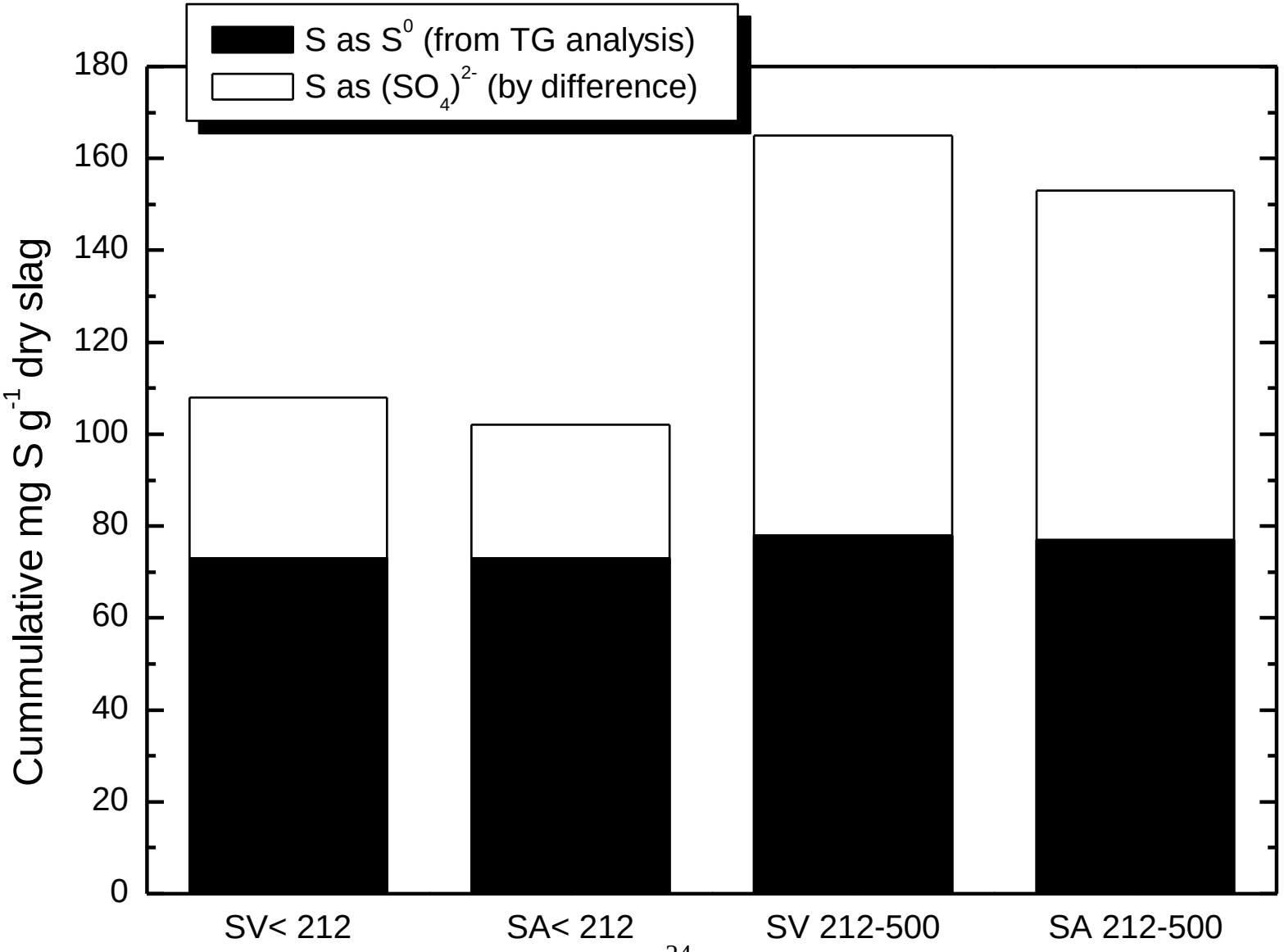
S as S^{0} (from TG analysis)
S as (SO$_4$)$^{2-}$ (by difference)
Cummulative mg S g^{-1} dry slag
0
20
40
60
80
100
120
140
160
180
SV< 212
SA< 212
SV 212-500
SA 212-500

FIGURE SI1

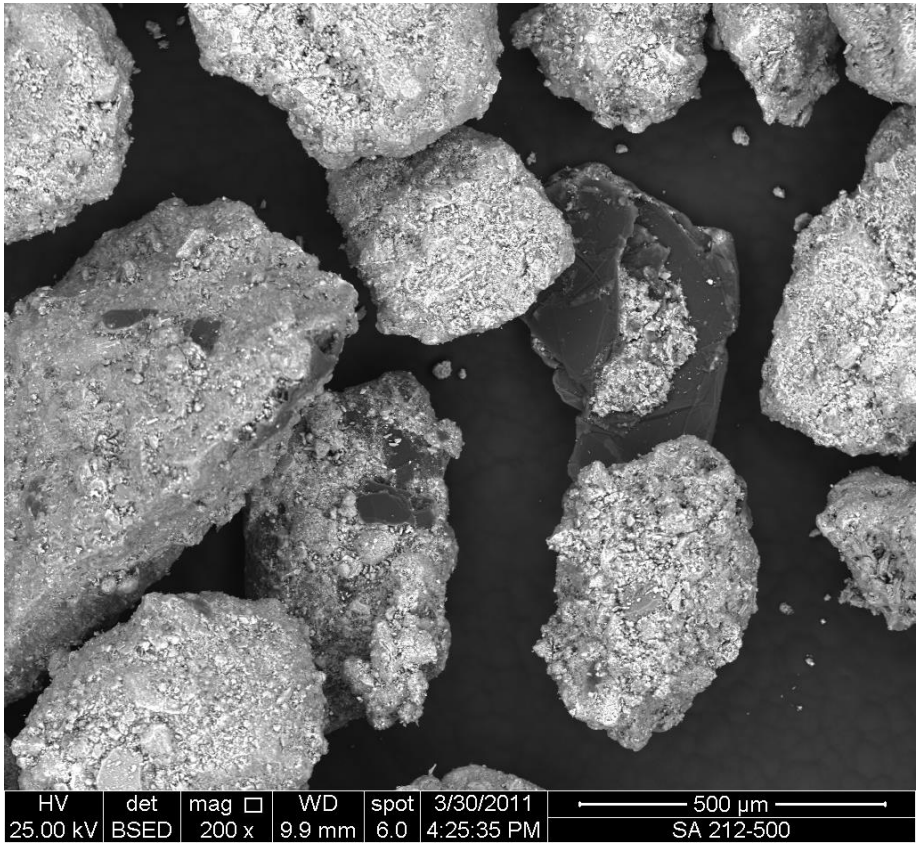
HV
25.00 kV
det
BSED
mag
200 x
WD
9.9 mm
spot
6.0
3/30/2011
4:25:35 PM
500 µm
SA 212-500

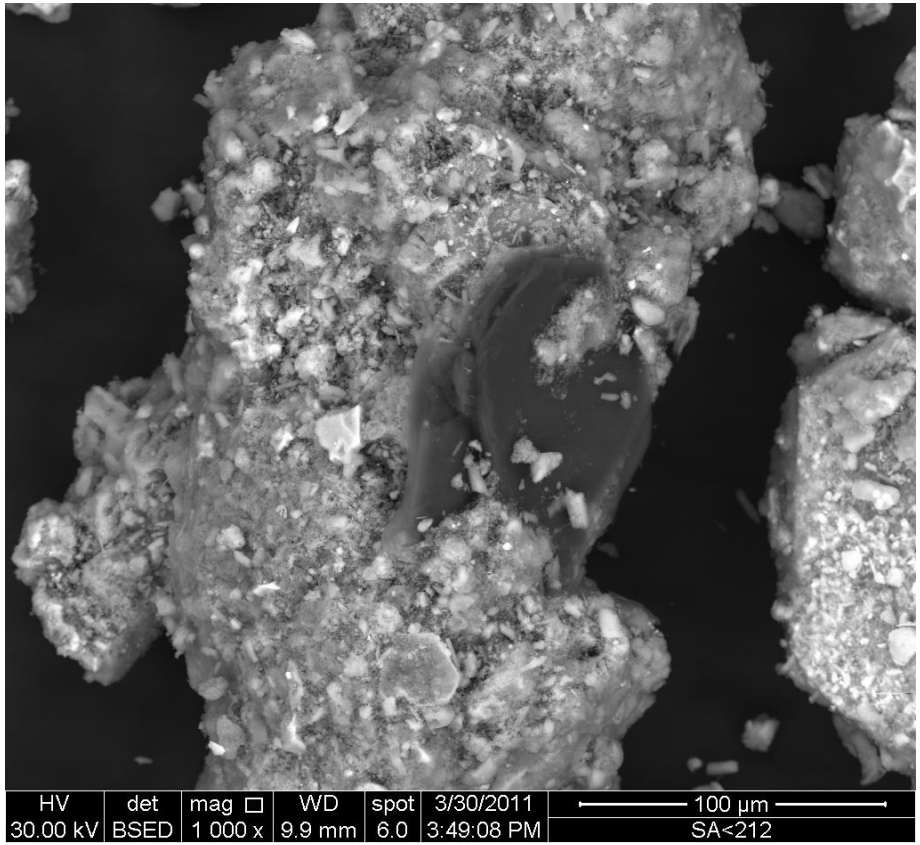
HV
30.00 kV
det
BSED
mag
1 000 x
WD
9.9 mm
spot
6.0
3/30/2011
3:49:08 PM
100 µm
SA<212

FIGURE SI2

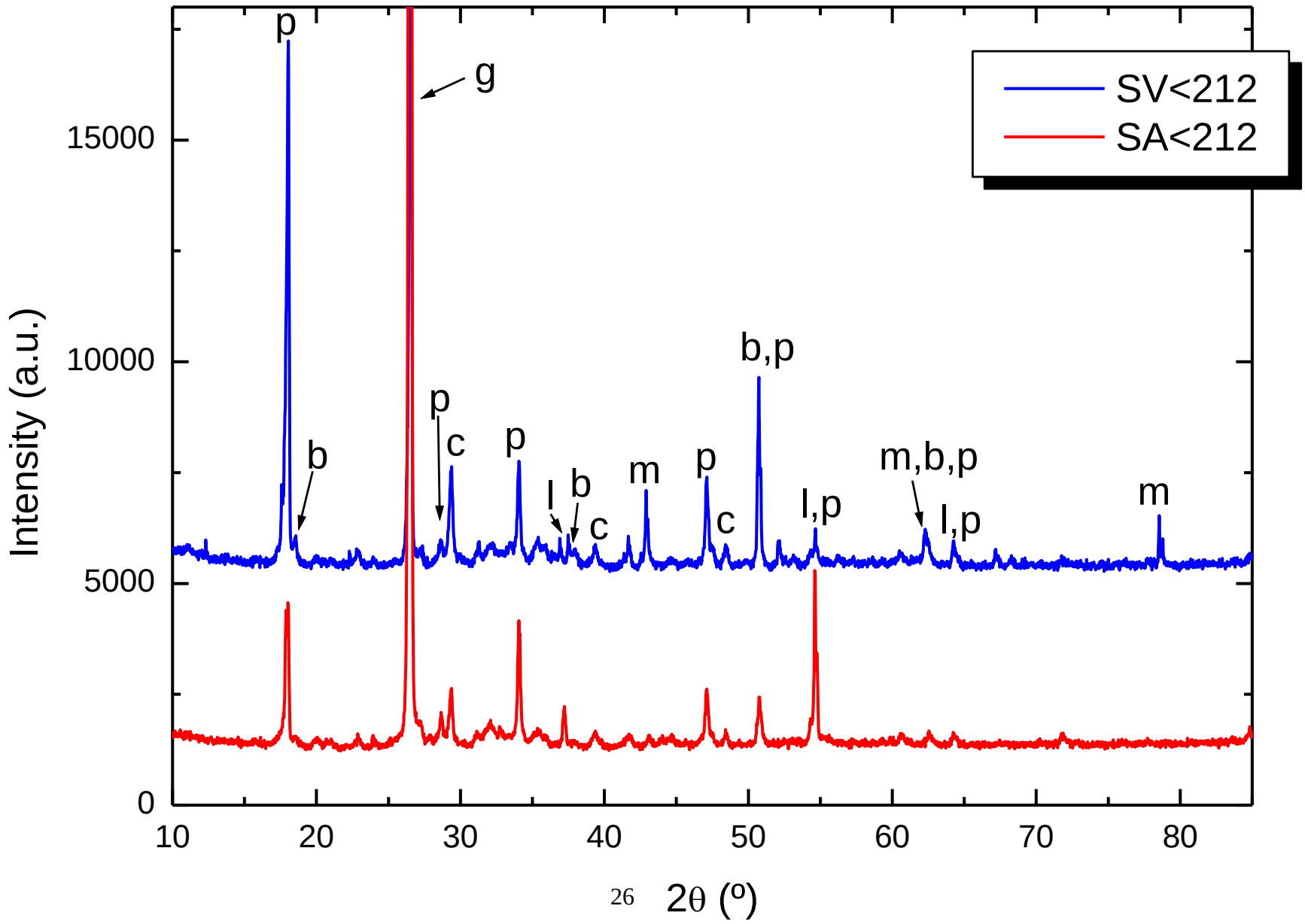
SV<212
SA<212
Intensity (a.u.)
0
5000
10000
15000
10
20
30
40
50
60
70
80
2θ (º)
p
g
b
p
c
p
l
b
c
m
p
c
b,p
l,p
m,b,p
l,p
m

FIGURE SI3

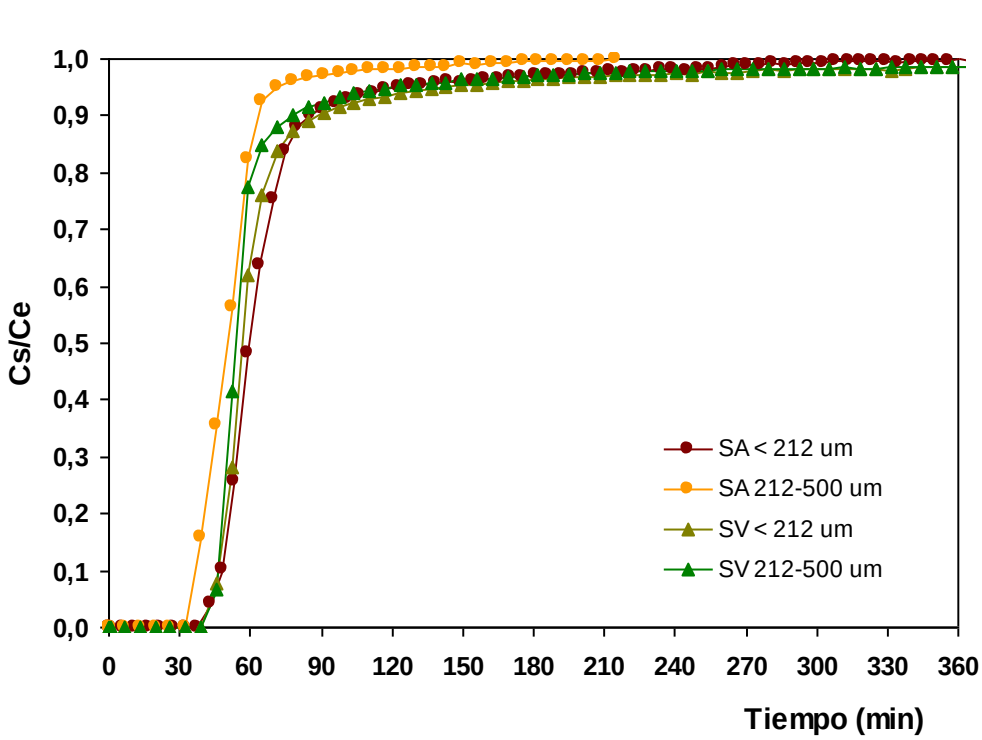
Cs/Ce
1,0
0,9
0,8
0,7
0,6
0,5
0,4
0,3
0,2
0,1
0,0
0
30
60
90
120
150
180
210
240
270
300
330
360
Tiempo (min)
SA < 212 um
SA 212-500 um
SV < 212 um
SV 212-500 um

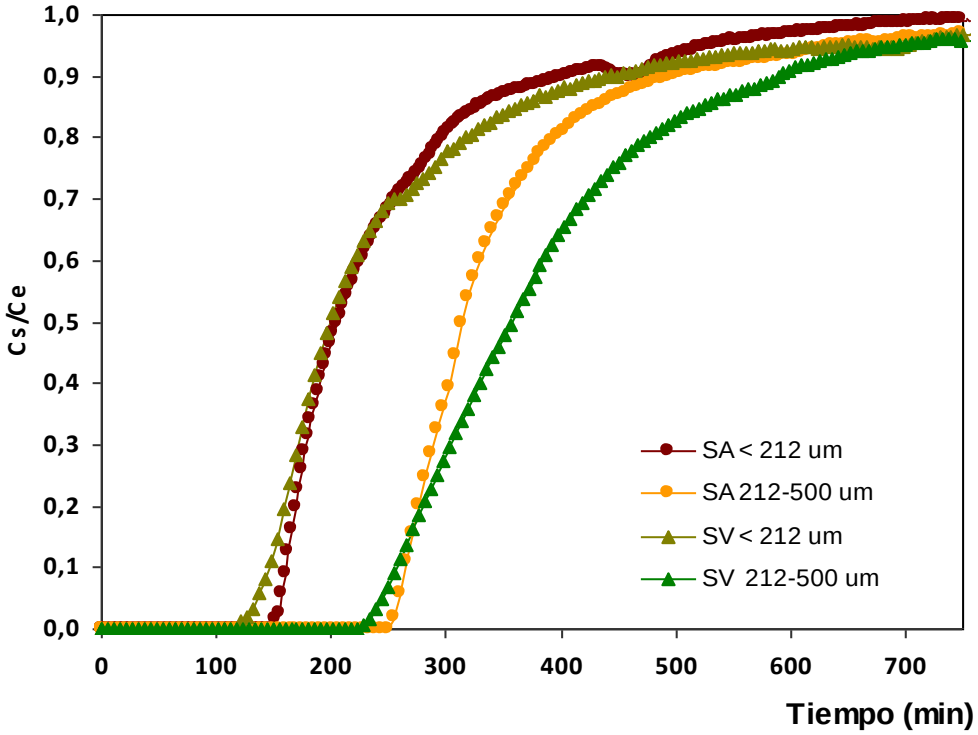
Cs/Ce
1,0
0,9
0,8
0,7
0,6
0,5
0,4
0,3
0,2
0,1
0,0
0
100
200
300
400
500
600
700
Tiempo (min)
SA < 212 um
SA 212-500 um
SV < 212 um
SV 212-500 um

FIGURE SI4

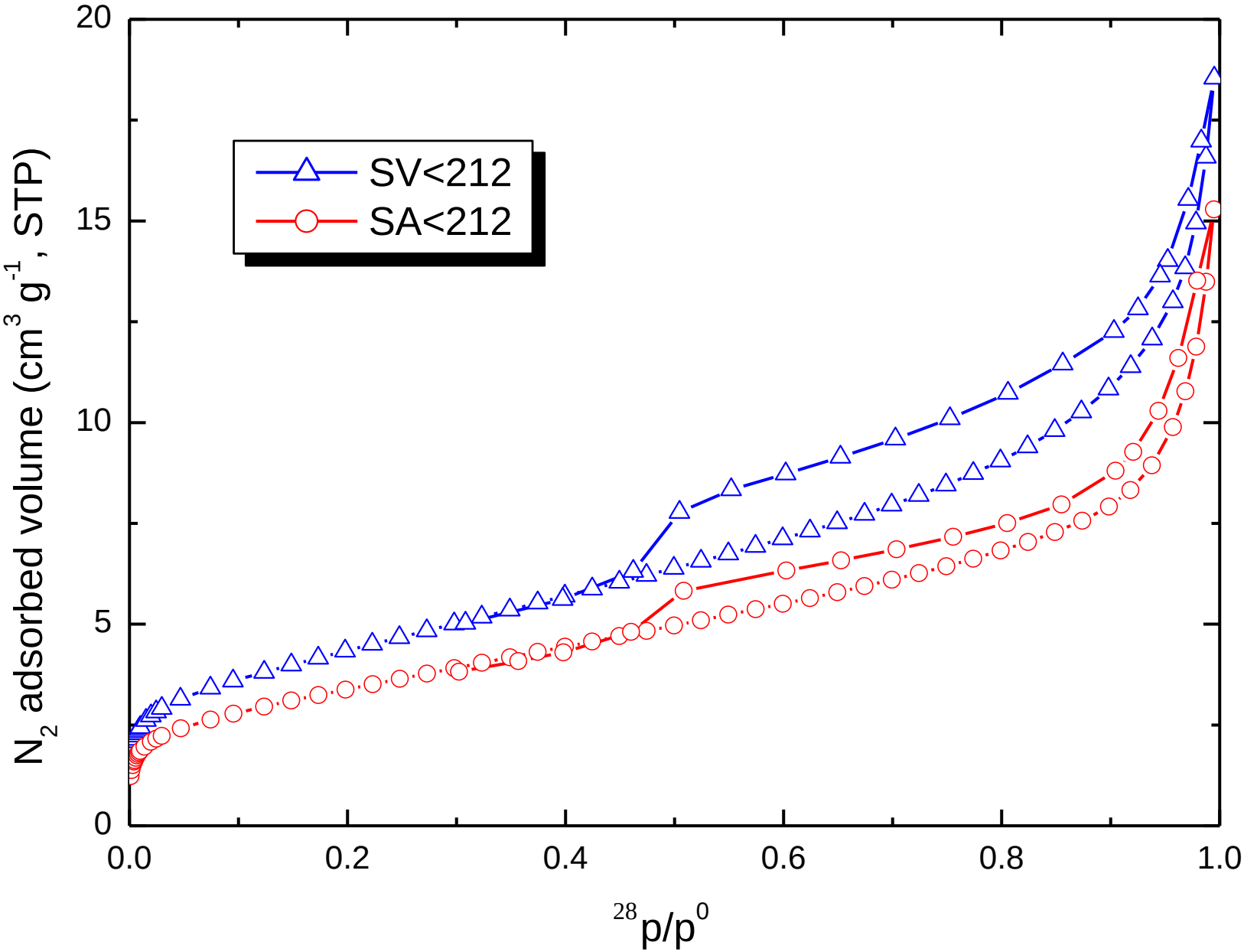
SV<212
SA<212
N2 adsorbed volume (cm3 g-1, STP)
28p/p0
0
5
10
15
20
0.0
0.2
0.4
0.6
0.8
1.0

FIGURE SI5

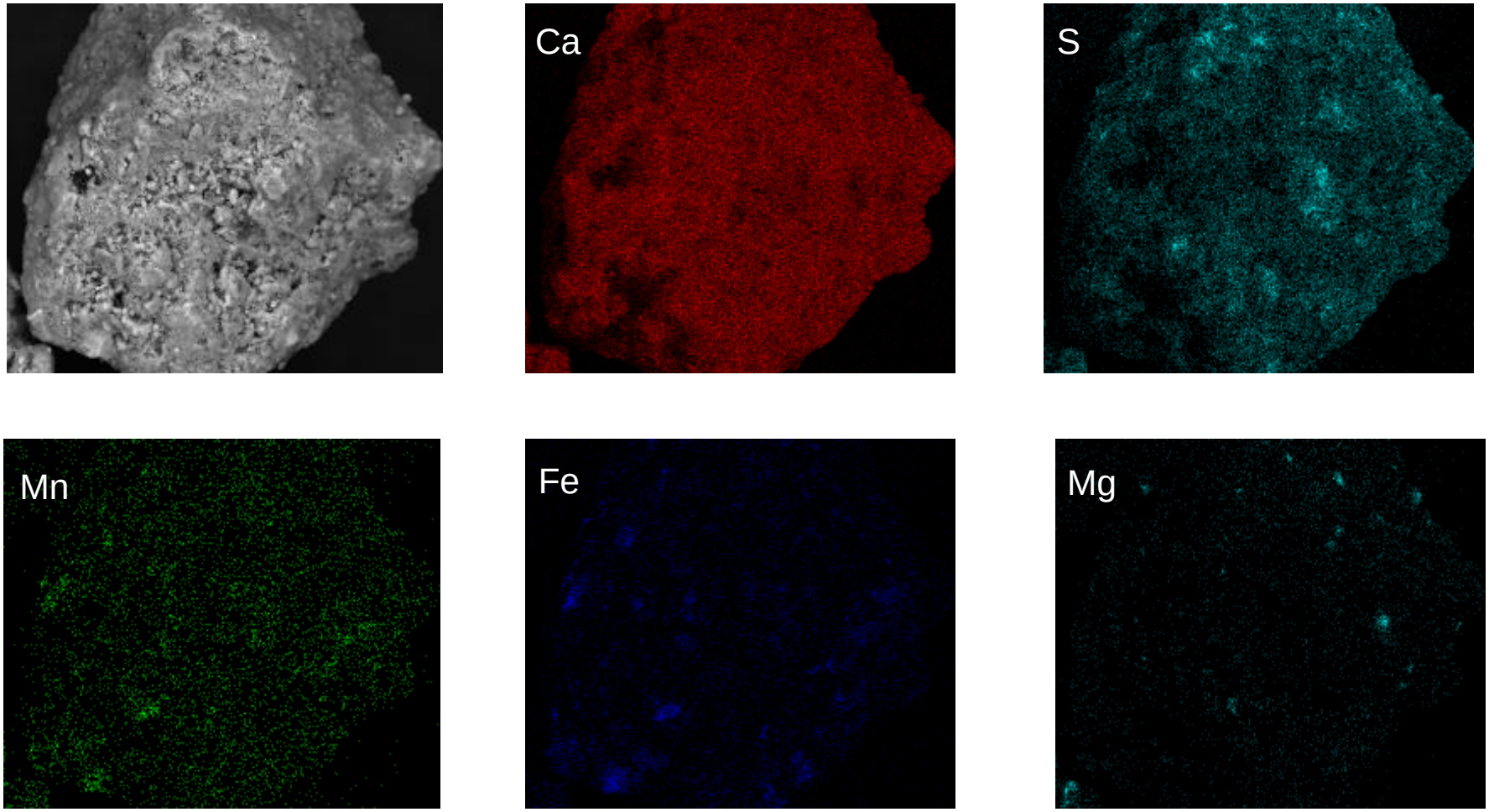

FIGURE SI6

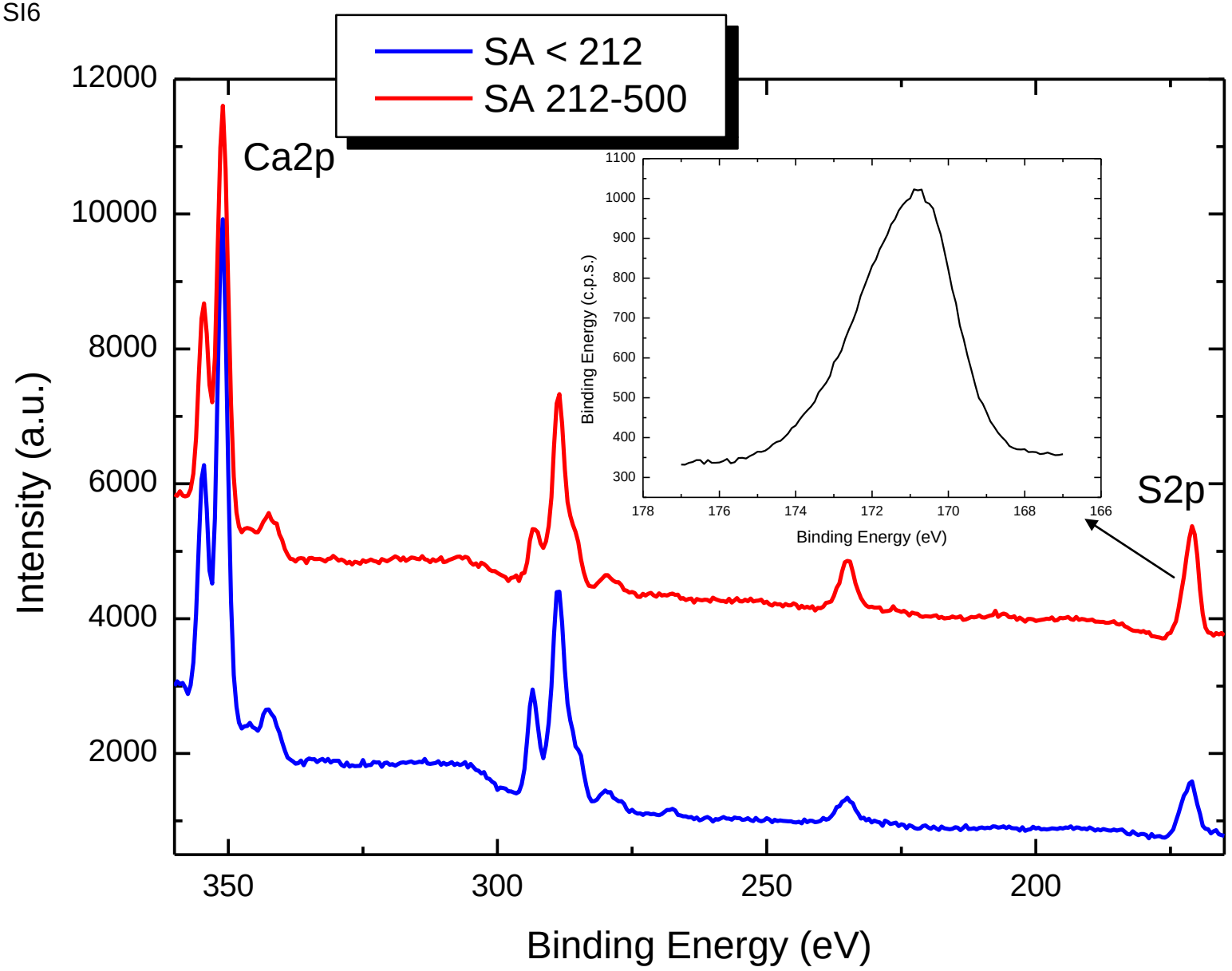
SA < 212
SA 212-500
Ca2p
S2p
Intensity (a.u.)
Binding Energy (eV)
12000
10000
8000
6000
4000
2000
350
300
250
200
Binding Energy (c.p.s.)
1100
1000
900
800
700
600
500
400
300
178
176
174
172
170
168
166
Binding Energy (eV)

FIGURE SI7

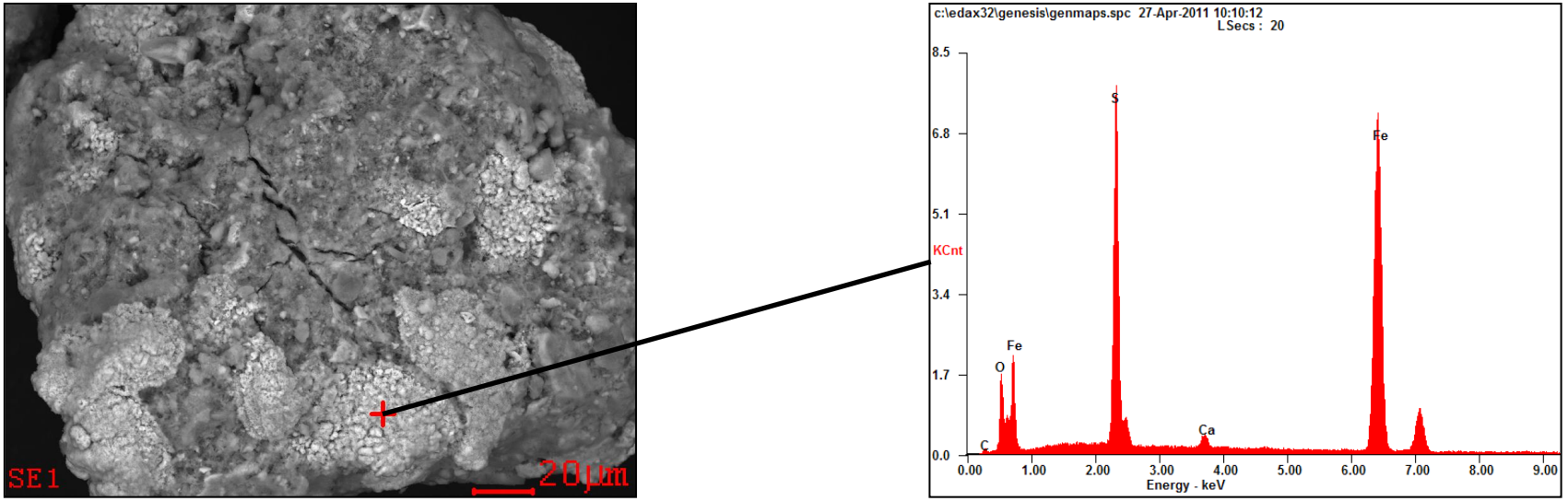
SE1
20µm
c:\edax32\genesis\genmaps.spc 27-Apr-2011 10:10:12
LSecs : 20
KCnt
Energy - keV
C
O
Fe
S
Ca
Fe

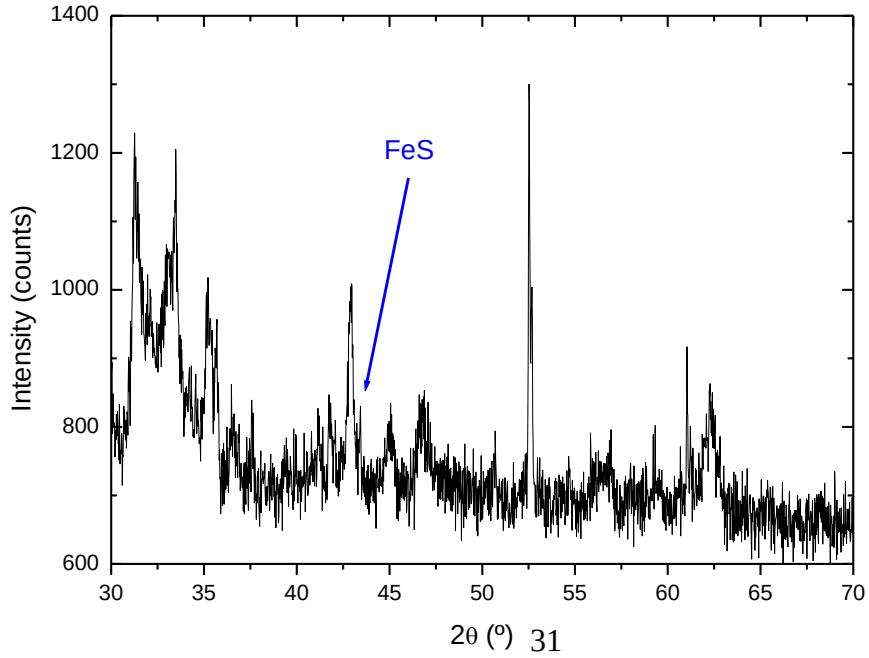
FeS
Intensity (counts)
2θ (º)